CrossMark

Incipient boninitic arc crust built on denudated mantle: the Khantaishir ophiolite (western Mongolia)

Omar Gianola[1] · Max W. Schmidt[1] · Oliver Jagoutz[2] · Oyungerel Sambuu[3]

Abstract The ~ 570 Ma old Khantaishir ophiolite is built by up to 4 km harzburgitic mantle with abundant pyroxenites and dunites followed by ~ 2 km of hornblende-gabbros and gabbronorites and by a ~ 2.5 km thick volcanic unit composed of a dyke + sill complex capped by pillow lavas and some volcanoclastics. The volcanics are mainly basaltic andesites and andesites (or boninites) with an average of 58.2 ± 1.0 wt% SiO_2, $X_{Mg} = 0.61 \pm 0.03$ (X_{Mg} = molar $MgO/(MgO + FeO^{tot})$, $TiO_2 = 0.4 \pm 0.1$ wt% and $CaO = 7.5 \pm 0.6$ wt% (errors as 2σ). Normalized trace element patterns show positive anomalies for Pb and Sr, a negative Nb-anomaly, large ion lithophile elements (LILE) concentrations between N- and E-MORB and distinctly depleted HREE. These characteristics indicate that the Khantaishir volcanics were derived from a refractory mantle source modified by a moderate slab-component, similar to boninites erupted along the Izu-Bonin-Mariana subduction system and to the Troodos and Betts Cove ophiolites. Most strikingly and despite almost complete outcrops over 260 km², there is

no remnant of any pre-existing MORB crust, suggesting that the magmatic suite of this ophiolite formed on completely denudated mantle, most likely upon subduction initiation. The architecture of this 4–5 km thick early arc crust resembles oceanic crust formed at mid ocean ridges, but lacks a sheeted dyke complex; volcanic edifices are not observed. Nevertheless, low melting pressures combined with moderate H_2O-contents resulted in high-Si primitive melts, in abundant hornblende-gabbros and in a fast enrichment in bulk SiO_2. Fractional crystallization modeling starting from the observed primitive melts (56.6 wt% SiO_2) suggests that 25 wt% pyroxene + plagioclase fractionation is sufficient to form the average Khantaishir volcanic crust. Most of the fractionation happened in the mantle, the observed pyroxenite lenses and layers in and at the top of the harzburgites account for the required cumulate volumes. Finally, the multiply documented occurrence of highly depleted boninites during subduction initiation suggests a causal relationship of subduction initiation and highly depleted mantle. Possibly, a discontinuity between dense fertile and buoyant depleted mantle contributes to the sinking of the future dense subducting plate, while the buoyant depleted mantle of the future overriding plate forms the infant mantle wedge.

✉ Omar Gianola
  omar.gianola@alumni.ethz.ch

1   Institute of Geochemistry and Petrology, ETH Zurich, Clausiusstrasse 25, 8092 Zurich, Switzerland

2   Department of Earth, Atmospheric, and Planetary Sciences, MIT, Cambridge, MA 02139, USA

3   School of Geology and Petroleum Engineering, Mongolian University of Science and Technology, Ulaanbaatar, Mongolia

Introduction

Oceanic crust amounts to nearly 60% of the Earth's surface and differs from the (on bulk average) andesitic continental crust by its basaltic composition, its higher density, its younger age (mostly ≤ 180 Ma) and its lesser thickness.

More than 90% of the oceanic crust is produced at mid-oceanic ridges (MOR), which have an average magma production of ~ 21 km^3/year, with 3 km^3/year being emplaced as volcanic rocks on seafloor (Crisp 1984). Some oceanic crust is also created in supra-subduction zone settings (e.g. Dilek and Furnes 2014), predominantly in back-arc basins of intra-oceanic subduction zones. However, the processes and implications related with the initiation of subduction in intra-oceanic domains are still matter of debate and different tectonic models have been proposed. The two major scenarios that seem to be more suitable for subduction initiation along intra-oceanic arcs invoke a spontaneous or an induced origin (Stern 2004). Induced subduction initiation is mainly related to external factors, such as polarity reversal, slab pull or ridge-push (e.g. Gurnis et al. 2004; Stern 2004), whereas spontaneous subduction occurs presumably at transform faults/fracture zones, when an old, denser oceanic plate collapses spontaneously into the asthenosphere and sinks below a young and buoyant lithosphere (Stern 2004). Several studies have suggested that the Izu-Bonin-Mariana (IBM) subduction system is an outstanding location to investigate subduction initiation and the evolution of an oceanic arc (e.g. Stern and Bloomer 1992; Stern 2004; Reagan et al. 2010; Ishizuka et al. 2011; Arculus et al. 2015).

From a magmatic point of view, melts erupted in supra-subduction settings range from tholeiitic and calc-alkaline basalts to rhyolites. Arcs also produce high-SiO$_2$ melts with primitive character, typically referred to as high-Mg andesites (e.g. Kelemen et al. 2003). One particular type of high-Mg andesites are boninites with SiO$_2$ > 52 wt%, MgO > 8 wt%, TiO$_2$ < 0.5 wt% (Le Bas 2000) and fairly depleted heavy rare earth elements (HREE, e.g. Pearce et al. 1992). Their depleted nature suggests an origin from a refractory harzburgitic mantle (e.g. Hickey and Frey 1982; Walker and Cameron 1983; Crawford et al. 1989). Boninites can be further subdivided into two broad subgroups, low-Ca boninites (CaO/Al$_2$O$_3$ < 0.75) and high-Ca boninites (CaO/Al$_2$O$_3$ > 0.75), which may inform on the mantle source that produced these magmas (e.g. Crawford et al. 1989; Cooper et al. 2010). Specifically, high-Ca boninites are thought to be produced from a mantle that is slightly less refractory (i.e. has a higher modal abundance of cpx) than low-Ca boninites. Although the key localities for boninites are nowadays in the Izu-Bonin forearc (Bonin Islands), these boninites are 48–44 Ma old (Cosca et al. 1998; Ishizuka et al. 2006) and have been erupted onto MOR-like tholeiitic basalts (referred as forearc basalts, Reagan et al. 2010; Ishizuka et al. 2011) during subduction initiation of the IBM system. Boninites in Tonga occur in a rear-arc position, i.e. in active submarine volcanoes located in proximity to the main volcanic arc (Resing et al. 2011) but even in the active arc (Cooper et al. 2010). Boninites have also been recognized in several ophiolitic complexes such as Troodos (Robinson et al. 1983;

Cameron 1985), the Alley volcanic unit of northern Oman (Ishikawa et al. 2002) and the Ordovician Betts Cove ophiolite (Bédard 1999), indicating that they have been formed in, or at least at one point related to, a supra-subduction zone setting (e.g. Shervais 2001).

This study focuses on the high-Mg basaltic andesite to andesitic volcanic upper crust of the Neoproterozoic Khantaishir ophiolite with the aim to (1) present the architecture of this arc crust with high-Mg andesitic composition, (2) constrain the geochemistry, parent liquid and liquid line of descent of this unusually Si-rich ophiolite suite, (3) understand the tectonic setting in which this arc crust formed and (4) draw implications for the initial arc building at the onset of intra-oceanic subduction.

Geology of the Khantaishir ophiolite

The ~ 570 Ma old Khantaishir ophiolite in western Mongolia is one of a dozen major ophiolitic bodies on the Mongolian territory (Fig. 1a). These ophiolites represent former oceanic domains that were, through a series of collisions, incorporated into the Central Asian Orogenic Belt (CAOB). The CAOB is one of the largest accretionary orogens in the world (Şengör et al. 1993), built over several hundred Myr and extending from the Urals to the Okhotsk Sea. Tectonically, the Khantaishir ophiolite is part of the Lake Terrane (Badarch et al. 2002), a remnant of the Paleo-Asian Ocean, which in turn represents a residual portion of the Paleo-Pacific Ocean (Ruzhentsev and Burashnikov 1996).

The Khantaishir ophiolite covers an area of ~ 260 km^2 and displays a rock association similar but not identical to a "Penrose-model" stratigraphy (Conference Participants 1972), with peridotites at the bottom overlain by gabbroic rocks and an extrusive sequence that includes a dyke + sill complex and pillow lavas, but lacks a sheeted dyke layer. According to Matsumoto and Tomurtogoo (2003) the Khantaishir may be subdivided into the Taishir massif to the West and the Naran massif to the East (Fig. 1b). The Naran massif exposes the largest and least serpentinized mantle portion (~ 4 km thick), whereas the crustal section is relatively thin, on average ~ 0.8 km of gabbros and ~ 0.5 km of volcanic rocks (Fig. 2). On the other hand, the western Taishir massif has a mantle section of on average only ~ 2 km, overlain by ~ 1.8 km of gabbros and ~ 2.5 km of volcanics (Fig. 2). The mantle of both massifs is mainly composed of harzburgites, with minor lenses and channels of dunite. These peridotites are over large areas moderately serpentinized (30–40 vol%), but in part completely transformed into tectonized serpentinites. In the uppermost 100–700 m of the Khantaishir mantle the modal abundance of pyroxenes increases upwards, culminating in a massive 50–200 m thick layer of websterites (with minor clino- and orthopyroxenites)
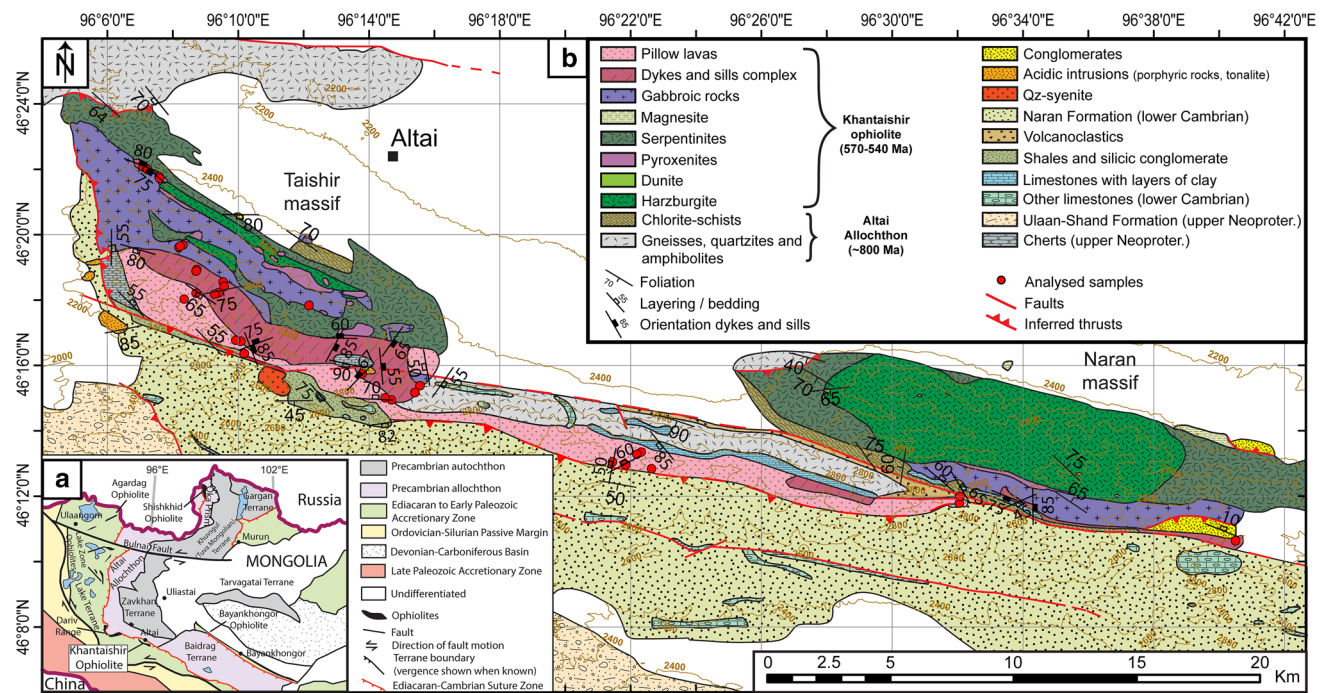
Fig. 1 **a** Tectonic overview of western Mongolia (modified from Bucholz et al. 2014). **b** Geological map of the Khantaishir ophiolite
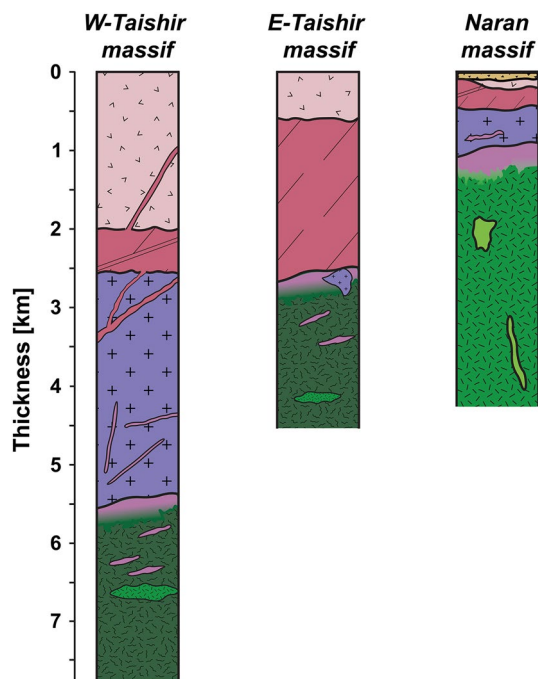

Fig. 2 Stratigraphic sections of the Naran and Taishir massifs (colors same as in Fig. 1)

at the contact to the gabbroic lower crust. Moreover, the Taishir mantle contains numerous tens of meters thick, hundreds of meters wide lenses of pyroxenites, which are sub-parallel to the Moho.

The lower crust of the Khantaishir is formed predominantly by a suite of isotropic hornblende gabbros and to a lesser extent by gabbronorites and few tonalites. The dominant minerals in the gabbroic rocks are plagioclase, amphibole, clinopyroxene (cpx) and orthopyroxene (opx) associated with minor chromite and magnetite. The thickness of the lower crust varies drastically along strike, from zero (i.e. volcanics directly on the mantle) to a maximum thickness of ~ 3 km. In the eastern Naran massif, the magmatic contact between the gabbroic lower crust and the underlying ultramafics is mostly exposed. In the Taishir massif, the ultramafic rocks are sometimes in direct contact with the lavas of the volcanic section without evidence of any major faulting. In their lower part, the gabbros of the ophiolite are intruded by dykes and sills of pyroxenite and/or dolerite, whereas the upper part is cut by volcanic dykes. Moreover, thin dykes (10–50 cm) of plagiogranites can be observed within the gabbros, where they locally form magmatic breccias.

The upper crust is characterized by a dyke + sill complex overlain by pillow lavas. The whole ophiolite sequence is then capped by red and green cherts, various carbonates (sometimes containing early Cambrian archaeocyathic fossils), volcanic sediments of unknown age and conglomerates. To the South, the ophiolite is thrusted under the lower Cambrian Naran Formation (mainly terrigenous sediments) and the Neoproterozoic Ulaan-Shand Formation (dominated by volcanoclastic). Intrusions of tonalites, granites and syenites, varying from 0.01 to 1.5 km in size, occur in the western Naran formation. The largest of these bodies

is a quartz-syenite stock, 1×1.5 km in size that is cut by the reverse fault (see Ruzhentsev and Burashnikov 1996) separating the Khantaishir ophiolite from the Naran Formation (see Fig. 1b). To the North the ophiolite is thrust onto the Altai Allochthon (Ruzhentsev and Burashnikov 1996), a metamorphic sequence that separates the Lake Terrane from the cratonic Zavkhan Terrane (Gibsher et al. 2001; Bucholz et al. 2014; Bold et al. 2016).

Geochronology

Limited geochronological data are available for the Khantaishir ophiolite. U–Pb zircon dating on plagiogranites yielded ages of 568 ± 4 and 573 ± 8 Ma (Gibsher et al. 2001; Jian et al. 2014). A similar U–Pb zircon age of 573 ± 6 Ma (Kozakov et al. 2002) was obtained for a plagiogranite from the Dariv oceanic crust (~ 100 km west of the Khantaishir), while a gabbro from the Bayankhongor ophiolite (~ 350 km East of the Khantaishir) has a Sm–Nd isochron at 569 ± 21 Ma (Kepezhinskas et al. 1991). By contrast, a U–Pb zircon age of 514 ± 8 Ma of an amphibolite outcropping between the base of the serpentinites of the Taishir massif and the metamorphic Altai allochthon is interpreted as the age of thrusting of the Khantaishir ophiolite onto the Zavkhan microcontinent (Jian et al. 2014; Bold et al. 2016). The amphibolitic metamorphism in Dariv was estimated to 490 ± 4 Ma (by U–Pb dating in zircons), while Ar–Ar-dating of metamorphic amphiboles in pillow basalts of the Bayankhongor provided an age of 485 ± 6 Ma (Delor et al. 2000).

Field and petrographical observations of the ophiolitic upper crust

The upper crustal section of the Khantaishir ophiolite is defined by a sequence of volcanic to hypabyssal dykes and sills capped by pillow lavas. In the West, the dyke + sill sequence is 1.0–1.8 km thick, but only 100–300 m in the East. Similarly, pillow lavas amount to 0.3–2.5 km in the west, while they are only 0.1–0.5 km thick in the East. Locally, the pillows of the Naran massif are not in direct contact with the dyke + sill complex but separated by a series of carbonates, volcanoclastics, plagioclase-bearing chlorite schists and other lithologies of the Altai-Allochthon, rendering the ophiolite somewhat dismembered in this part.

Volcanic dykes and sills, as well as pillow lavas, are aphanitic and relatively fresh, with a matrix consisting of plagioclase, cpx, magnetite and chromite. Occasionally the rocks show (hyp)idiomorphic phenocrysts of cpx (0.2–2.5 mm) and, more rarely, also plagioclase (~ 1 mm). Sometimes chlorite + spinel pseudomorphosis after olivine

and weathered pyrite phenocrysts may also be noticed. The characteristic thickness of the dykes and sills is 30–100 cm (Fig. 3a), and in the dykes, chilled margins are common (Fig. 3b). Sometimes gabbros or magmatic breccia with xenoliths of hornblendite occupy the inter-dyke space (Fig. 3c), in particular at the contact between lower crust gabbros and dykes of the volcanic section. Pillow lavas are characterized by dark red weathering colors and have typical diameters of 30–70 cm occasionally exceeding 1 m in size (Fig. 3d). Locally, pillows are cut by dykes of the dyke + sill complex (Fig. 3e). Vesicles, sometimes filled by secondary quartz or secondary calcite, are ubiquitous and can be used as "way-up" criteria. Based on the fact that vesicles tend to form at the surface of the pillow, where water first comes in contact with the lava, the sequence has a top-to-the-South orientation in agreement with the general stratigraphy. All volcanics from the upper crust are characterized by epidote and saussuritized plagioclase, indicative for greenschist-facies metamorphism. Furthermore, secondary veins of epidote, quartz and calcite can be observed across the entire volcanic section (Fig. 3f).

Volcanic dykes and sills are occasionally observed in the gabbroic section and even more rarely in the peridotitic mantle. The dykes and sills cutting the gabbros may display chilled margins and may occur in association with dykes and (sporadic) sills of dolerite. Dolerites are mainly found within the gabbroic section and the dykes + sills complex. They have an ophitic-intergranular texture and consist of strongly saussuritized plagioclase (40 vol%), quartz (12 vol%), cpx (7 vol%) and minor oxides, and of abundant greenschist minerals such as actinolite (34 vol%), chlorite (6 vol%) and epidote (1 vol%). Lavas from the dykes + sills complex and from the pillow section have the same crystallization sequence of magnetite + chromite → cpx phenocrysts → plagioclase microphenocrysts + cpx microphenocrysts of the groundmass.

On the other hand, dolerites have a similar crystallization sequence, showing magnetite + chromite → cpx phenocrysts → plagioclase → quartz.

Dykes or sills are discriminated based on their orientation with respect to the bedding observed in the cherts. In the field, the cherts overlying the volcanic section of the ophiolite are oriented 61/024 (dip/dip direction). The dykes from the dyke + sill complex display two conjugate directions: With respect to the cherts rotated into a horizontal position, one group is oriented 63/287[1] on average, the other 68/128; similar to the volcanic dykes cutting the pillow lavas (39/273 and 47/176) or the gabbroic crust (51/295 and 45/192). The

---

[1] The following averages are all rotated: stereoplots and the original measurements (Online Resource 1 and Online Resource 9) are provided in the Electronic Appendix.

Fig. 3 The upper crust of the Khantaishir ophiolite. **a** Steeply inclined dykes. **b** Contact between two dykes with the dyke on the right showing a chilled margin. **c** Magmatic breccia with angular xenoliths of hornblendite filling the inter-dyke space in the dyke and sill complex. **d** Pillow lavas. **e** Dyke cutting pillow lavas. **f** Secondary veins of epidote + quartz + calcite within the volcanic section of the ophiolite
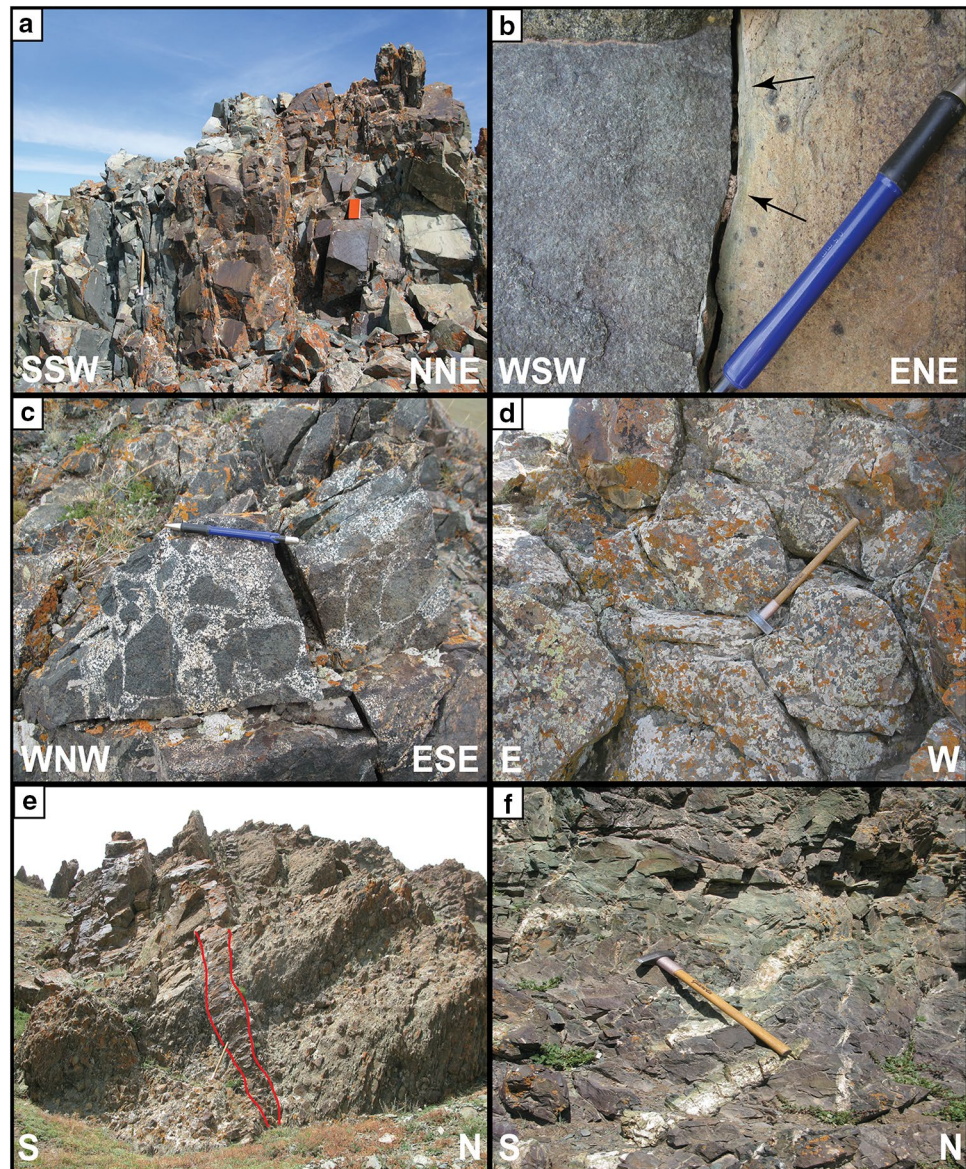
rotated average orientation of the sills in the dyke + sill complex is 19/215, similar to the volcanic sills in the gabbros (with 11/232). The dyke + sill complex is dominated by dykes, while sills amount to 15–20% of the outcrops. The doleritic dykes intruding the upper ultramafic section of the ophiolite define three (rotated) average directions: 45/127, 63/302 and 56/231. The majority of the "beddings" noticed in the pillow lavas dips towards NW with an average of 24/314, only few directions dip to the SW (average: 37/207).

The presence of sills associated with the dykes and a general dip of 50°–60° for these latter suggests that the Khantaishir dyke + sill complex is not equivalent to a classical vertical sheeted dyke complex as, for example, exposed in the Oman ophiolite.

In the Naran massif 200–300 m of volcanoclastics are in tectonic contact with both pillow lavas to the South and carbonates to the North. Volcanoclastics are very fine-grained and consist of quartz, plagioclase, abundant chlorite and some epidote.

Analytical methods

Samples were powdered with an agate mill and dried overnight in an oven at 105 °C. About 2 g of powder was heated at 1050 °C for 2 h and weighted again to determine the loss of ignition (LOI). Subsequently, the rock powders were mixed with di-Lithium tetraborate ($Li_2B_4O_7$) in a 1:5 ratio ($5 \times Li_2B_4O_7$) and fused into glass discs. X-ray fluorescence (XRF) analyses of major elements were carried out at the Institute of Geochemistry and Petrology at ETH Zurich

with a wavelength dispersive XRF spectrometer (Axios of PANanalytical).

Laser ablation inductively coupled mass spectrometer (LA-ICP-MS) measurements of trace elements were also performed at ETH using a laser ablation unit with a 193 nm ArF Excimer laser from Lamda Physics. Fresh broken fragments of the XRF glass discs were mounted in the ablation cell, together with an external glass standard (NIST 610) and a di-Lithium tetraborate blank, from where the ablated material was transported to the ICP-MS by a gas mixture of Ar–He. A typical cycle of analysis included two measurements of the NIST 610 standard: one measurement of the blank and 7–8 sample measurements, each glass disc being analyzed at least 3 times. The laser ablation beam aperture was 40 μm for the external standard and 90 μm for blank and samples. The measured intensities were then converted into concentrations with the SILLS program (Guillong et al. 2008), with the concentration of CaO determined by XRF used as an internal standard. Complete bulk rock chemical analyses and respective locations for Khantaishir samples are listed in the Online Resource 10.

Bulk rock compositions

According to the boninite classification of Crawford et al. (1989), volcanic and hypabyssal rocks of the Khantaishir ophiolite can be subdivided into low-Ca boninites, high-Ca boninites and an andesitic suite. The volcanic rocks of the Khantaishir ophiolite are mainly basaltic andesites to andesites, with few dacites (Online Resource 2a) and have SiO_2-contents mostly ranging from 53 to 65 wt%. In the AFM diagram, the volcanic and hypabyssal rocks follow a trend that starts in the tholeiitic field (with high-Ca boninites) but, instead of evolving towards the FeO-corner straddle the tholeiitic—calc-alkaline boundary, where the majority of low-Ca boninites and andesites plot (Fig. 4). In K_2O–SiO_2 space[2] the volcanic rocks evolve in the arc tholeiite field (Peccerillo and Taylor 1976, Online Resource 2b). The volcanics have bulk X_{Mg} (defined as molar MgO/$(MgO + FeO^{tot})$ ranging from 0.80 to 0.38 (Fig. 5a–f). The highest X_{Mg} values are observed for two dykes having a high-Ca boninite composition, whereas low-Ca boninites have bulk X_{Mg} mainly between 0.75 and 0.60. On the other hand, most of the high-Mg andesites belonging to the andesitic suite have $X_{Mg} < 0.64$. In the dykes, sills and volcanoclastic rocks CaO decreases with decreasing X_{Mg}, while SiO_2, Na_2O
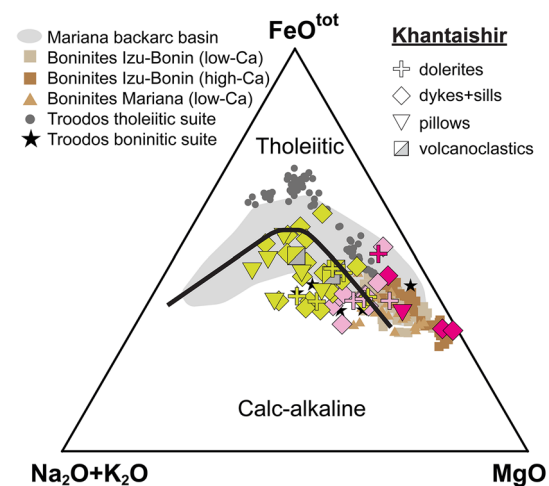

Fig. 4 AFM diagram for volcanic and hypabyssal rocks of the Khantaishir ophiolite. Color shading for the Khantaishir: magenta = high-Ca boninites, pink = low-Ca boninites and yellow = high-Mg andesites of the andesitic suite. Data for the Mariana backarc basin and Izu-Bonin-Mariana boninites are from GEOROC (http://georoc.mpch-mainz.gwdg.de/georoc) and PetDB (http://www.earthchem.org/petdb). Data for the Troodos ophiolite were compiled from König et al. (2008) and Regelous et al. (2014)

and TiO_2 increase with fractionation. Al_2O_3 remains nearly constant at 15 wt % for andesites, but decreases with increasing X_{Mg} for low-Ca and high-Ca boninites. By contrast, K_2O does not increase much with differentiation. Pillow lavas overlap the field of dykes and sills but are somewhat lower in SiO_2 at a given X_{Mg}. Dolerites and volcanoclastic rocks have restricted ranges of X_{Mg} of 0.74–0.58 and 0.59–0.49 respectively, major element concentrations overlap those of the dykes and sills. Dolerites are mainly subdivided into andesites and low-Ca boninites, whereas volcanoclastic rocks belong to the andesite suite.

Trace elements (Fig. 6a–f) outline an increase of V and Zr with fractionation, whereas Sc, Ni and Cr decrease with melt evolution. The majority of the volcanic and volcanoclastic rocks have Sr concentrations between 10 and 80 ppm, whereas in dolerites Sr increases with decreasing X_{Mg}.

Trace element patterns (Fig. 7a–c) normalized to primitive mantle (McDonough and Sun 1995) show that the primitive to slightly fractionated volcanic rocks ($X_{Mg} = 0.80$–0.60) have most trace element concentrations similar to primitive mantle: 0.5–1 orders of magnitude less than MORBs. Most rocks show positive Pb and Sr anomalies (with respect to REE), a negative Nb-anomaly as well as a slight enrichment in large ion lithophile elements (LILE; Cs, Rb, Ba) and in U. The more evolved rocks ($X_{Mg} < 0.60$) are enriched in LILE, Th, U and in REEs. Together with a clear Nb-anomaly they display variable attitudes for Pb and Sr, with negative and positive anomalies for both elements.

---

[2] One volcanic dyke is a completely un-metamorphosed alkali basalt (KT12-53, Electronic Appendix), not co-genetic to the rest of the suite. In analogy to other volcanism in the area it may be of tertiary age.
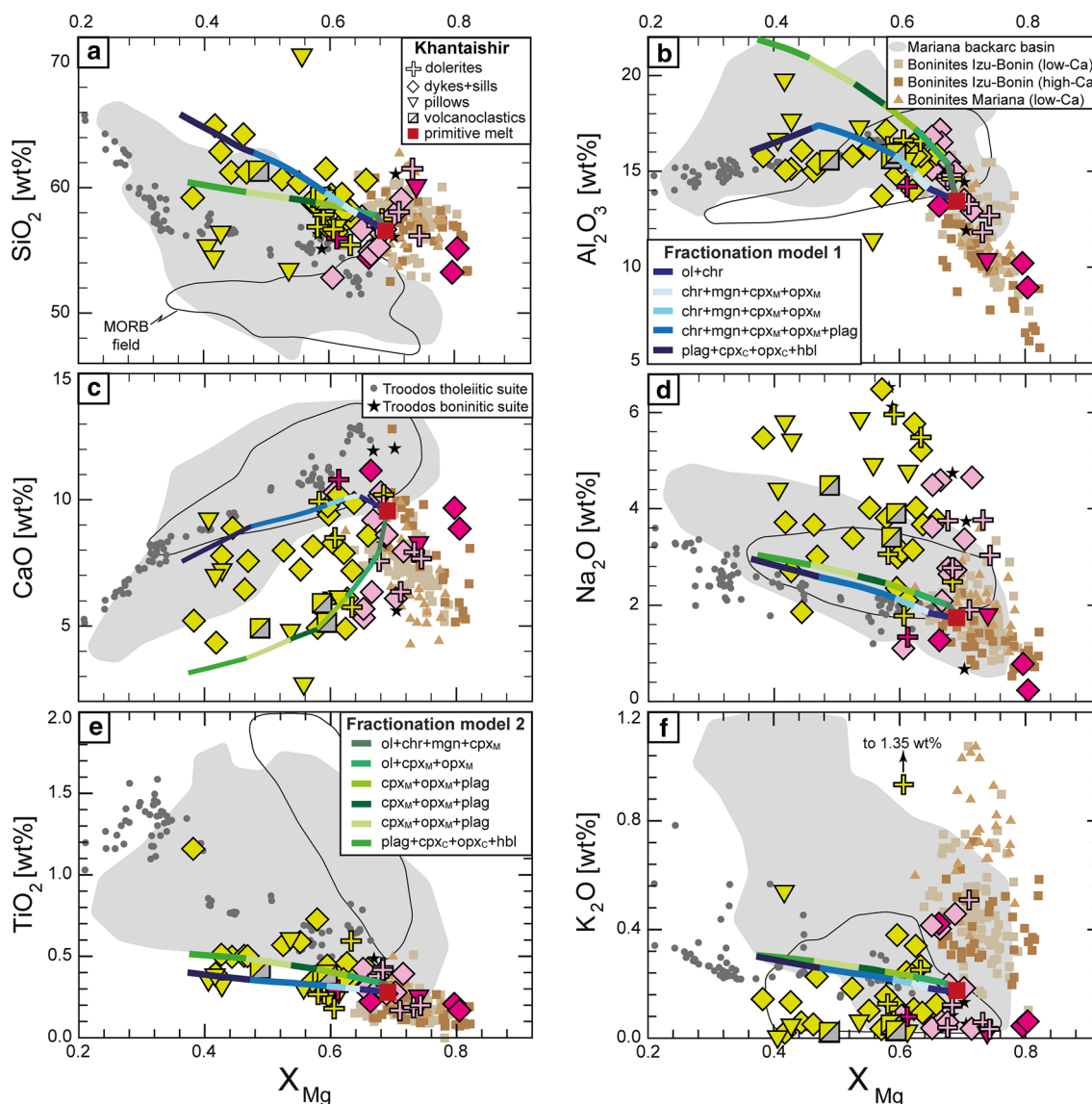
Fig. 5 Bulk major elements (normalized to 100% on anhydrous basis) for the volcanic and hypabyssal rocks of the Khantaishir ophiolite. Color shading for the Khantaishir: magenta = high-Ca boninites, pink = low-Ca boninites and yellow = high-Mg andesites of the andesitic suite. Primitive melt composition as defined in section "The primitive melt parental to the boninite-suite" and reported in Table 1. Data for the East Pacific Rise (EPR), the Mariana backarc basin and Izu-Bonin-Mariana boninites are from GEOROC and PetDB. Data for the Troodos ophiolite were compiled from König et al. (2008) and Regelous et al. (2014)

The REE patterns of the Khantaishir ophiolite (Fig. 7a–c, REE alone in Online Resource 3) are characterized by La_N/Sm_N = 0.47–9.38 for dolerites, 0.38–4.08 for dykes and sills and 0.24–0.77 for pillows, while Dy_N/Yb_N is 0.37–0.97 for dolerites, 0.50–2.14 for dykes and sills and 0.60–1.04 for pillow lavas. The volcanoclastics are comparable to dykes/sills and pillow lavas, with La_N/Sm_N and Dy_N/Yb_N of 0.92–1.11 and 0.83–0.95, respectively.

Stratigraphic chemical variations within the Khantaishir ophiolite upper crust have not been observed; there is neither a discernible vertical nor lateral systematics in the dyke + sill complex and the pillows (see Online Resource 4 and Online Resource 5).

Discussion

The upper crust of the Khantaishir ophiolite, defined by the dyke + sill complex, dolerites, pillow lavas and volcanoclastics, is made of basaltic andesites to andesites with strongly depleted trace element patterns that have (1) high field strength elements (HFSE) at primitive mantle levels
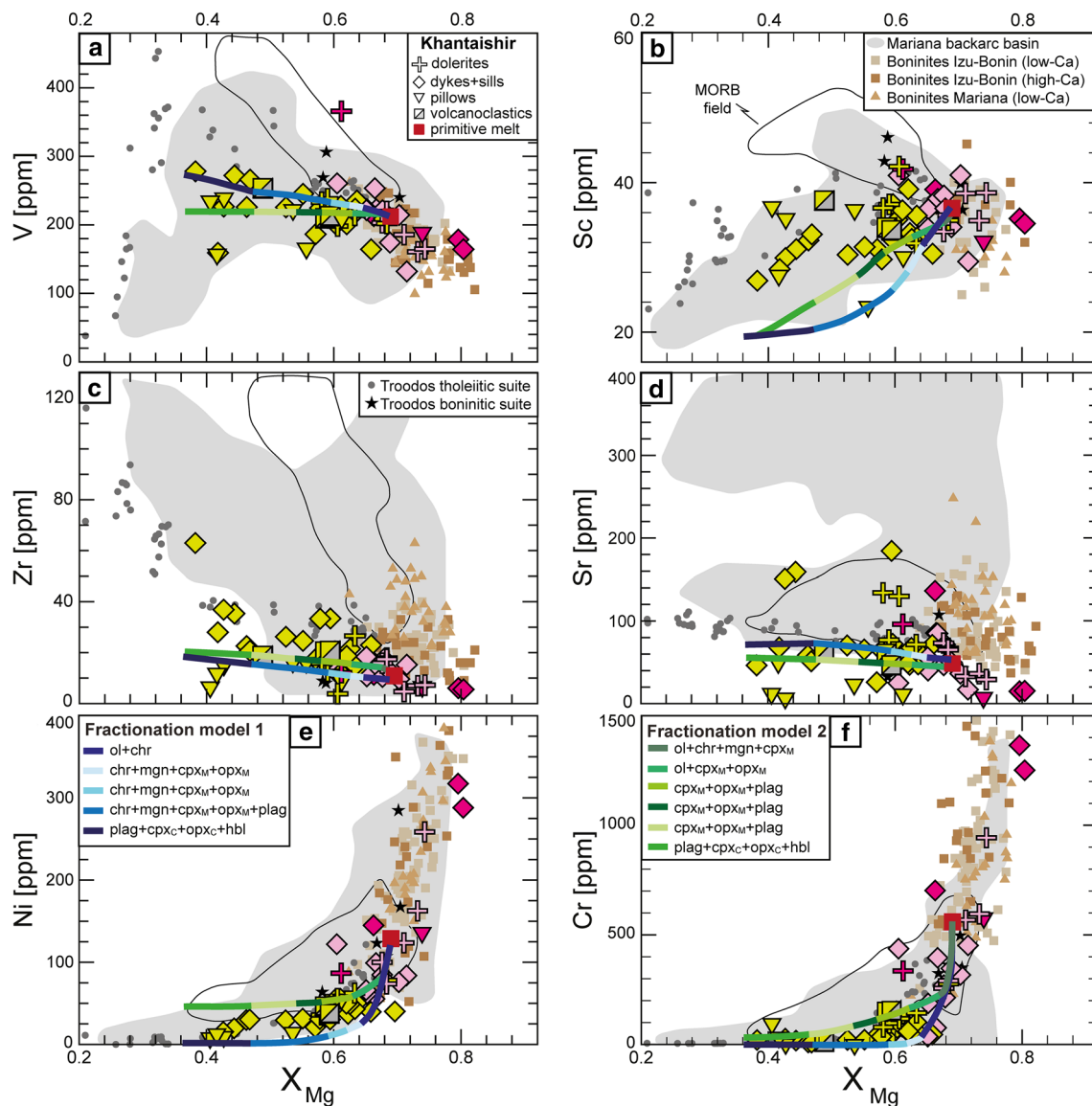
Fig. 6 Bulk trace elements for the volcanic and hypabyssal rocks of the Khantaishir ophiolite. Color shading: magenta = high-Ca boninites, pink = low-Ca boninites and yellow = high-Mg andesites of the andesitic suite. Primitive melt composition as defined in section "The primitive melt parental to the boninite-suite" and reported in Table 1.

Data for the East Pacific Rise (EPR), the Mariana backarc basin and Izu-Bonin-Mariana boninites are from GEOROC and PetDB. Data for the Troodos ophiolite were compiled from König et al. (2008) and Regelous et al. (2014)

and (2) a moderate slab component expressed in increased LILE, a negative Nb-anomaly and (for most samples) positive Pb- and Sr-anomalies. The identical chemical composition in both major and trace elements between dolerites and andesitic dykes/sills indicates that dolerites were formed by andesitic melts that had enough time to cool down and to form a coarser-grained matrix than the other lavas.

In the following sections, we will discuss the impact of hydrothermal metamorphism, identify the parent melt of this magma suite, model the liquid line of descent and discuss modern analogues and the tectonic situation in which the

basalt-andesitic to andesitic crust of the Khantaishir ophiolite formed.

Evaluation of the hydrothermal metamorphism

Similar to other ophiolitic complexes (see review by Gillis and Banerjee 2000), the volcanic rocks of the Khantaishir ophiolite are overprinted by low greenschist-facies metamorphism. This metamorphism is mainly characterized by the presence of saussuritized plagioclase, actinolite and epidote. The lack of massive metasomatism (leading, e.g.
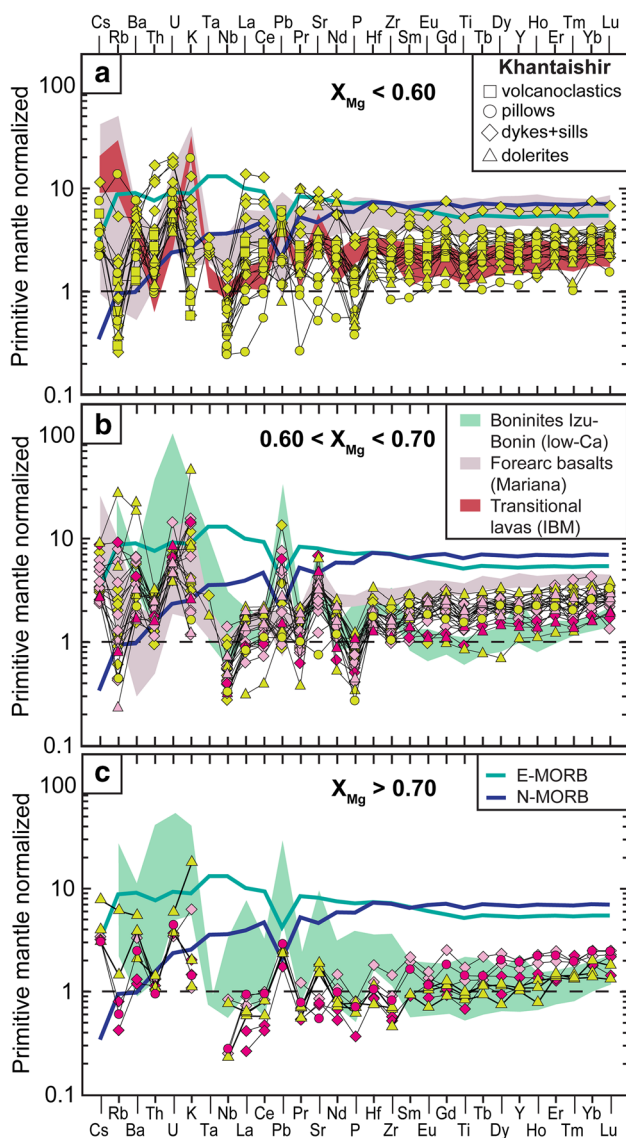
Fig. 7 Trace element normalized patterns for the volcanic rocks of the Khantaishir ophiolite. **a** X_{Mg} < 0.60. **b** 0.60 < X_{Mg} < 0.70. **c** X_{Mg} > 0.70. Color shading: magenta = high-Ca boninites, pink = low-Ca boninites and yellow = high-Mg andesites of the andesitic suite. The field for the Izu-Bonin boninites (data from GEOROC and PetDB), the Mariana forearc basalts (Reagan et al. 2010), the IBM transitional lavas (Reagan et al. 2010) and the patterns for N-MORB and E-MORB (Sun and McDonough 1989) are also plotted as reference

to rodingites) suggests that the circulating fluids were limited in volume but it remains unclear whether the overprint occurred at the oceanic floor and/or during the obduction of the ophiolite. The effects of extensive plagioclase saussuritization may be recognized in the large scatter displayed by Na_2O (Fig. 5d). The dispersion in Na_2O concentrations is analogous to the one observed in the boninitic suite of the Troodos ophiolite (König et al. 2008) and, therefore, is interpreted to derive from magmatic differentiation.

Nevertheless, it cannot be excluded that some samples from the Khantaishir ophiolite (especially the high-Mg andesites) may have suffered minor Na-enrichment, due to the albitization of Ca-rich plagioclase. By contrast, most of the analyzed rocks have lower K_2O concentrations than typical boninites from the IBM arc (except for one dolerite showing a clear K-enrichment by fluids, Fig. 5f), suggesting that greenschist metamorphism in the Khantaishir ophiolite may have removed some K to different extents (leading to some scattering in the variation diagram). This can be also recognized in normalized trace element patterns, where K is mostly depleted compared to typical low-Ca boninites with similar X_{Mg} intervals (and for some samples even depleted than primitive mantle values). Other mobile elements, such as Pb and Sr, show random positive and negative anomalies (especially Pb) in the normalized trace patterns. However, we notice that there is no systematic enrichment or depletion between the different lithologies (i.e. boninites and high-Mg andesites), suggesting that Pb (and partially for Sr) may have been locally redistributed at outcrop-scale. Furthermore, the dominant positive anomalies for Pb and Sr vary in the range observed for boninites and forearc basalts dredged along the IBM subduction system. It is, therefore, assumed that these positive anomalies are primary magmatic and not the result of alteration processes.

The primitive melt parental to the boninite-suite

Melts in equilibrium with mantle olivine and chromite have X_{Mg} = 0.65–0.74 (at Fe^{3+}/Fe^{tot} = 0.2) and Ni and Cr contents of 100–500 and 300–1100 ppm, respectively. Two dykes from the dyke + sill complex (KTB-4 and KT11-83) and one pillow lava (KTP-1) yield calculated equilibrium olivines with X_{Mg} = 0.89–0.92 (using Roeder and Emslie 1970) employing Fe^{3+}/Fe^{tot} = 0.2 as characteristic for near-primitive arc basalts (e.g. Kelley and Cottrell 2009). Calculated $Ni^{olivine}$ varies within 2200–3400 ppm, using a temperature of 1100 °C and the equation of Li and Ripley (2010). These ranges are comparable to those of olivines from the harzburgitic mantle of the Khantaishir ophiolite, where $Ni^{olivine}$ is 2400–3400 ppm and X_{Mg} = 0.92–0.93 (Gianola, unpubl. data).

These three primitive samples are tholeiitic high-Mg andesites with on average 56.5 ± 4.0 wt% SiO_2, $Na_2O + K_2O$ = 1.9 ± 0.7 wt%, FeO^{tot} = 8.0 ± 1.2 wt% and MgO = 10.0 ± 1.2 wt% (Table 1 and Online Resource 11). This composition lies in the range of the boninites of the Khantaishir ophiolite (Figs. 5, 8). In projection from diopside they fall into the quartz-normative field of the basalt tetrahedron (Fig. 9; Ulmer 2001), similar to primitive boninites recovered from Expedition 352 at site U1439 (Reagan et al. 2015). Pressure contours of the olivine-opx cotectic on the (Jd + CaTs + Lc)–Ol–Qz surface for 3 wt% H_2O

Table 1 Averaged bulk rock compositions (normalized to 100% on anhydrous basis)

	Khantaishir ophiolite lithologies				Primitive compositions		
	Dyke and sill complex	Pillow lavas	Dacitic lavas	Average volcanic crust[a]	Khantaishir	High-Ca boninites[b]	Mariana BAB
Majors (wt%)							
N	26	6	3	43	3	10	27
SiO_2	57.46	56.49	66.71	57.11	56.54	55.75	50.95
TiO_2	0.41	0.40	0.41	0.40	0.28	0.23	0.80
Al_2O_3	15.08	16.39	13.89	15.74	13.43	12.03	16.05
FeO^{tot}	7.62	8.51	6.73	8.08	7.97	8.36	8.09
MnO	0.13	0.15	0.07	0.14	0.16	0.13	0.15
MgO	7.89	5.86	3.43	6.74	9.98	11.04	9.81
CaO	7.93	7.28	4.54	7.49	9.59	10.32	11.16
Na_2O	3.21	4.72	4.11	4.07	1.73	1.67	2.10
K_2O	0.17	0.14	0.05	0.14	0.17	0.43	0.71
P_2O_5	0.04	0.03	0.05	0.03	0.02	0.02	0.18
X_{Mg}	0.627	0.523	0.479	0.570	0.690	0.701	0.682
Traces (ppm)							
Cs	0.08	0.07	0.08	0.07	0.10	0.30	0.21
Rb	1.29	1.79	0.25	1.49	2.23	8.59	6.97
Ba	24.82	22.33	17.07	22.57	18.82	31.28	122.40
Th	0.20	0.09	0.26	0.14	0.10	0.70	0.46
U	0.13	0.11	0.15	0.12	0.12	1.70	0.18
Ta	0.08	–	0.11	0.04	–	0.02	0.08
Nb	0.44	0.21	0.48	0.31	0.24	0.92	2.82
La	1.05	0.50	1.35	0.76	0.54	1.68	5.16
Ce	3.03	1.75	3.70	2.34	1.49	2.52	10.28
Pb	0.41	0.45	0.21	0.43	0.54	0.97	2.03
Pr	0.42	0.24	0.52	0.33	0.19	0.47	1.56
Sr	59.11	22.01	49.61	38.27	77.27	106.09	303.79
Nd	2.45	1.64	2.96	2.01	1.16	1.44	7.36
Hf	0.62	0.57	0.79	0.58	0.46	0.51	1.28
Zr	18.36	12.98	22.95	15.23	11.06	23.25	67.49
Sm	0.92	0.89	0.96	0.89	0.60	0.58	2.20
Eu	0.34	0.28	0.35	0.30	0.21	0.23	0.80
Gd	1.36	1.22	1.46	1.27	0.96	0.98	2.62
Tb	0.24	0.20	0.24	0.22	0.16	0.15	0.47
Dy	1.72	1.59	1.90	1.63	1.31	1.18	2.84
Y	10.45	9.23	11.05	9.62	7.95	8.00	20.41
Ho	0.38	0.35	0.45	0.36	0.29	0.27	0.63
Er	1.23	1.17	1.22	1.18	0.94	0.81	1.81
Tm	0.18	0.14	0.20	0.16	0.12	0.14	0.27
Yb	1.30	1.26	1.21	1.26	0.98	0.78	1.74
Lu	0.20	0.17	0.21	0.18	0.15	0.12	0.27
Sc	34.33	33.70	28.24	34.00	36.58	39.37	35.11
V	217.01	217.27	185.85	215.71	210.09	186.38	218.73
Cr	255.78	156.29	15.17	204.94	563.58	870.83	493.16
Ni	80.51	47.32	25.79	63.27	129.42	212.37	187.39
Co	32.78	32.72	23.00	32.53	37.92	45.27	37.49

[a] Calculated using 36% of lavas from the dyke + sill complex + 55% of pillow lavas + 1% dacites + 5% dolerites + 3% volcanoclastics
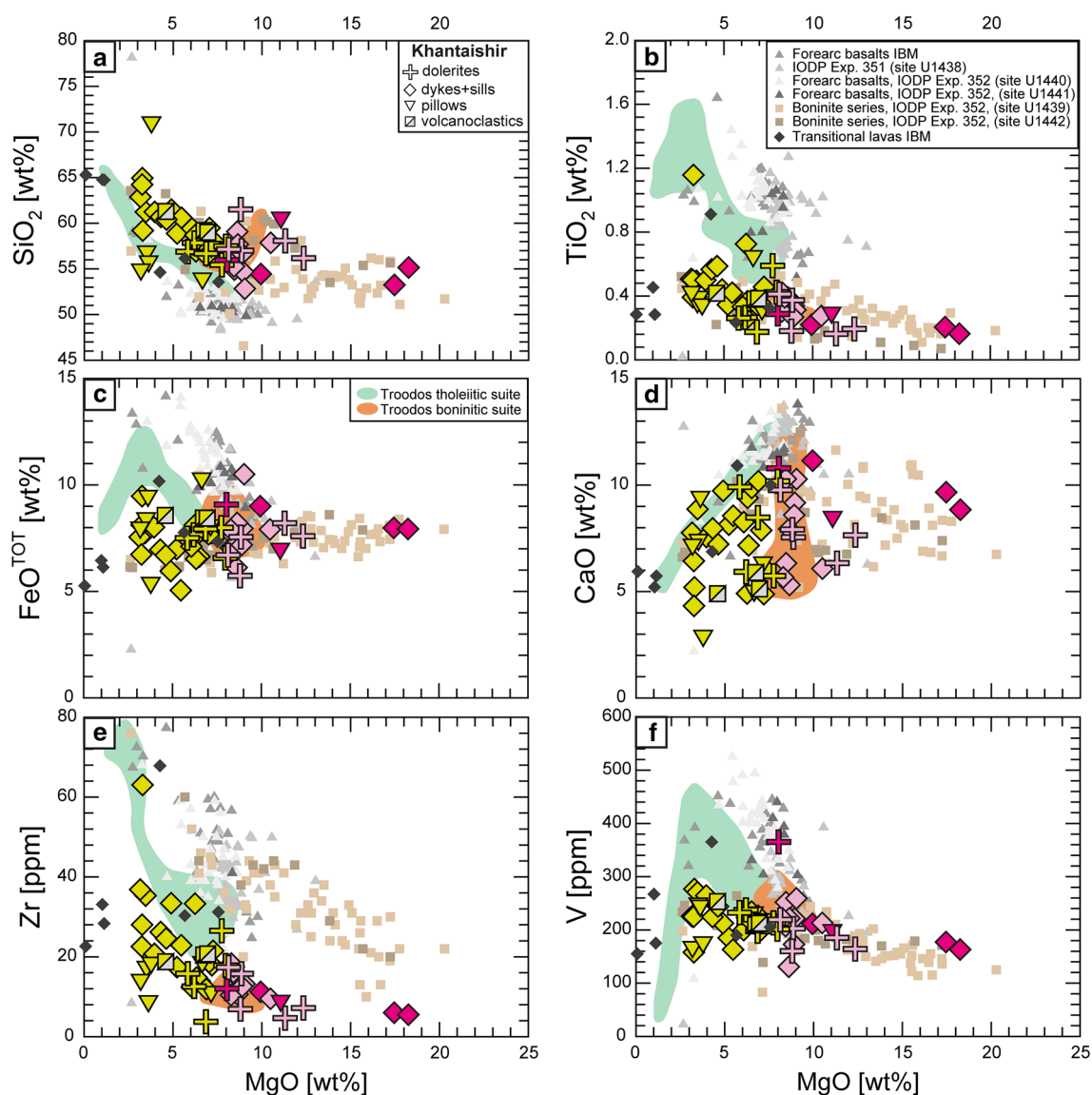
[b] Boninites from the Izu-Bonin arc

Fig. 8 Bulk major elements (normalized to 100% on anhydrous basis) and trace elements for the volcanic and hypabyssal rocks of the Khantaishir ophiolite plotted against MgO. Color shading for Khantaishir: magenta = high-Ca boninites, pink = low-Ca boninites and yellow = high-Mg andesites of the andesitic suite. Data for forearc basalts and transitional lavas are from Reagan et al. (2010). Data for IODP Expedition 351 are from Arculus et al. (2015) and data for IODP Expedition 352 are from Reagan et al. (2015). Data for the Troodos ophiolite were compiled from König et al. (2008) and Regelous et al. (2014)

(Ulmer 2001) indicate equilibrium with their mantle source at ≤ 1 GPa, possibly as low as 0.5 GPa. Nevertheless, this has to be taken with caution as pressure and H_2O have opposite effects, − 0.1 GPa being roughly equivalent to + 3 wt% H_2O.

Similar to the entire rock suite, the primitive melts have a moderate enrichment in LILE, negative anomalies for Nb, P and Zr and positive anomalies for Sr and Pb. These features, in particular the positive Sr or Pb, are hence not related to crystal fractionation or accumulation but derive directly from the subduction component. The Khantaishir primitive melts are notably different from those related to

mid-oceanic ridges and backarc basins (Online Resource 6a–c), but comparable to primitive melts from modern intra-oceanic subduction zones and the Troodos ophiolite (Online Resource 6b–d).

Original H_2O-contents cannot be quantified, but significant H_2O-concentrations are indicated by the preponderance of cpx phenocrysts over plagioclase (which is mainly observed in the groundmass), implying that plagioclase saturation was probably delayed by H_2O (Gaetani et al. 1993). Also, the crystallization of hornblende in the lower crustal gabbros suggests several wt% H_2O at this stage.
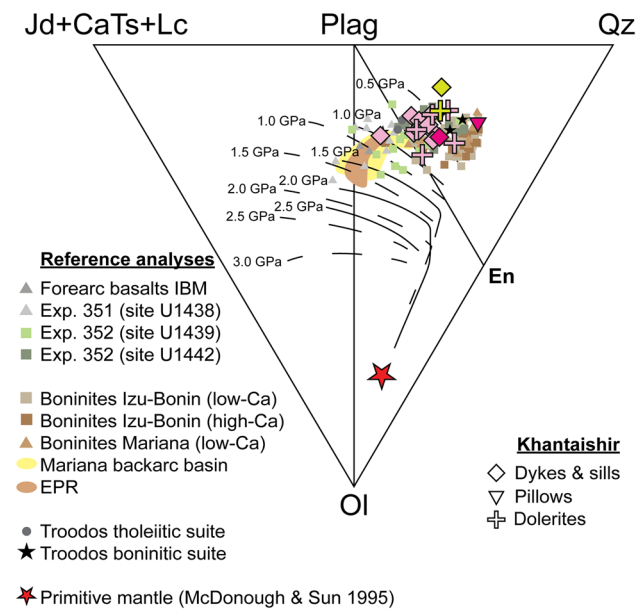
Fig. 9 Molecular normative projection from diopside onto the [Jd + CaTs + Lc]–Qz–Ol base of the basalt tetrahedron for volcanics and dolerites of the Khantaishir ophiolite. Primitive lavas for the EPR, the Mariana backarc basin and Izu-Bonin-Mariana are from GEOROC and PetDB. Data for forearc basalts and transitional lavas are from Reagan et al. (2010). Data for IODP Expedition 351 are from Arculus et al. (2015) and data for IODP Expedition 352 are from Reagan et al. (2015). Data for the Troodos ophiolite were compiled from König et al. (2008) and Regelous et al. (2014)

Experiments have shown that boninitic melts may be generated by H_2O-assisted melting of a harzburgitic refractory mantle at pressures between 0.3 and 2 GPa (e.g. Umino and Kushiro 1989; Van der Laan et al. 1989). At these pressures, peritectic melting of opx at elevated H_2O-contents leads to the formation of silica-rich melts similar to those observed in the Khantaishir ophiolite. This interpretation is supported by field observations, with the underlying harzburgitic mantle containing pyroxenite cumulates and lower crust gabbronorites containing abundant opx.

Fractional crystallization model

The primitive melt average and the upper crust volcanics are suitable to reconstruct the magma evolution and liquid line of descent of the Khantaishir ophiolite. In the absence of any contaminant, magma evolution is modeled by pure fractional crystallization, subtracting measured cumulate mineral compositions from the evolving melt (Figs. 5a–f, 6a–f). For this endeavor, we first use the more primitive mineral compositions of the abundant mantle pyroxenites and then those from cumulative pyroxenites, gabbros and gabbronorites of the lower crust (see Online Resource 12).

To cover the range of observed compositions, two fractional crystallization end-members were modeled

(Figs. 5a–f, 6a–f). One resulted in five, the other in six fractionation intervals. A new interval was set when the liquid lines of descent did not follow the analyzed data anymore. For both models and at every fractionation step, the X_{Mg} of olivine, cpx and opx in equilibrium with the melt are calculated [Kd (Fe–Mg)$_{Ol}$ = 0.30 (Roeder and Emslie 1970), Kd (Fe–Mg)$_{Cpx}$ = 0.23 (Sisson and Grove 1993) and Kd (Fe–Mg)$_{Opx}$ = 0.29 (Putirka 2008)] and appropriate observed mineral compositions selected, first from the mantle pyroxenites, then from the crustal pyroxenites and then from the gabbros and gabbronorites. Trace elements are modeled using partition coefficients from the literature (see Online Resource 13). Apart from a few compatible elements (such as Ni concentrated in olivine, Cr in chromite and Sc in cpx), most trace element concentrations increase moderately through passive enrichment with progressing fractionation. Several trace element trends have scatters that are almost as large as the enrichment through fractionation. One of the trace elements, Sr, is little constrained by its average concentration of 77.3 ± 72.6 ppm (2σ) in the primitive melt. Therefore, we adjusted the Sr concentration (48 ppm in model 1 and 45 ppm in model 2) by averaging only KTP-1 and KT11-83, such that the fractionation trend follows the majority of the volcanics.

Model 1 begins with the fractionation of olivine and chromite followed by two fractionation intervals with chromite, magnetite, cpx^{mantle} and opx^{mantle}. The fourth interval is similar to intervals 2 and 3, except for the additional fractionation of plagioclase. The fifth short interval involves crustal minerals (plagioclase, cpx^{crust}, opx^{crust} and amphibole). In total, there are 5.4 wt% of olivine fractionation (to decrease Ni in the melt until Ni is controlled by cpx), 8.6 wt% of chromite (delimited by Cr-concentrations in the parent magma), 1.6 wt% of magnetite, 18.0 wt% of cpx and 11.0 wt% of opx with mantle compositions, 13.3 wt% of plagioclase (1.3 wt% in the mantle and 12.0 wt% in the crust), 0.6 and 2.0 wt% of cpx and opx with crustal compositions and 3.2 wt% of amphibole.

The second fractionation model comprises a first interval with olivine, chromite, magnetite and cpx^{mantle}, a second interval with olivine, cpx^{mantle} and opx^{mantle}, intervals 3–5 with fractionation of cpx^{mantle}, opx^{mantle} and plagioclase in different proportions and a last interval with the same minerals but with crustal compositions. In total, there are 1.7 wt% of olivine fractionation, 0.2 wt% of chromite, 1.4 wt% of magnetite, 37.0 and 9.1 wt% of cpx and opx with mantle compositions, 3.5 wt% of plagioclase (1.9 wt% in the mantle and 1.6 wt% in the crust), 0.4 and 3.2 wt% of cpx and opx with crustal compositions and 3.6 wt% of amphibole.

The largest portion of the fractionation trends requires minerals from the mantle pyroxenites, suggesting that 46 (model 1) to 51 (model 2) wt% of crystals fractionate from the most primitive melt within the mantle. Fractionation at

crustal levels, leading to the more evolved rocks and generating cumulative gabbros, only accounts for 19.1 (model 1) and 8.8 wt% (model 2) of mineral subtraction. To yield the bulk composition of the upper Khantaishir crust (i.e. the average of volcanic and hypabyssal rocks, Table 1) only 25 wt% crystal fractionation are necessary, i.e. 14 wt% cpx, 8 wt% opx and 3 wt% plagioclase. The overall major element mass balance between the average of the primitive melts and the volcanics does not require olivine or chromite; nevertheless, small amounts (< 1 wt%) are necessary to reduce Ni and Cr concentrations. On average, the pyroxenites in the mantle amount to several hundred meters in thickness and the volcanics to 1.5–2.0 km. This implies that during this early stage of arc crust formation most of the fractionation occurs in the sub-adjacent lithospheric mantle, only the volumetrically minor more evolved rocks require further fractionation in the crust. The modeled end-members give a first-order approximation of the upper and lower boundaries in which the fractional crystallization processes affected the evolution of volcanic and hypabyssal rocks from the Khantaishir ophiolite. The sometimes large scatter observed in major and trace element concentrations suggests in fact that fractionation occurred along more than one liquid line of descent. Therefore, all the compositions that lie between the modeled curves should have fractionated the same mineral assemblages but with different mineral proportions. It has also to be noticed that the models strongly depend on the initial composition of the primitive melt and that a slight difference in its composition (for some elements just few ppm) may shift the modeled curves in a considerable manner.

Comparison to other rock suites

Mid ocean ridge (MOR) and backarc basin (BAB) suites

The elevated SiO_2-range and qtz-normative character of the Khantaishir crust strongly contrasts with mid-ocean ridge basalts (illustrated by the East Pacific Rise—EPR—suite, Fig. 5a) or backarc basin volcanics (illustrated by the Mariana BAB suite), which are olivine normative and less depleted in Jd + CaTs + Lc-component (Fig. 9). In major element diagrams, the Khantaishir is clearly set apart from mid ocean ridge generated crust not only by higher SiO_2 but also by lesser CaO and TiO_2, and opposite trends in Al_2O_3 with fractionation (Fig. 5a–f). The same is valid for backarc basin suites, which have major element concentrations similar to MORB.

The low concentrations in V, Sc and Zr in the Khantaishir volcanics (Fig. 6a–f) suggest that their mantle source was much more depleted than MORB mantle or the source mantle of backarc basin basalts. Also variations in Ti/V, Th–Nb–Yb and Ba/Th (Online Resource 7a–d) show that the tholeiitic high-Mg andesites of the Khantaishir are very

distinct from backarc basin or MOR-suites. The low Ti/V may indicate a source mantle more oxidized than that of the EPR or the Mariana backarc basalts. In summary, despite its oceanic crust-like architecture, the Khantaishir crust has no geochemical affinities to mid-ocean ridge or backarc basin suites.

Boninites and forearc basalts (FAB)

Low-Ca and high-Ca boninites from the Khantaishir ophiolite show major and trace elements variations similar to those observed in the low-Ca and high-Ca boninites from the IBM subduction system, in particular in their high SiO_2 and low CaO, Al_2O_3 and TiO_2 (Fig. 5a–f). All these suites are tholeiitic in K_2O–SiO_2 space (Peccerillo and Taylor 1976), but evolve towards the calc-alkaline field in the (Na, K)$_2$O–FeO–MgO space (AFM), a behavior that characterizes modern intra-oceanic arcs (e.g. Stern et al. 2003; Tatsumi and Suzuki 2009). On the other hand, high-Mg andesites from the andesitic suite of the Khantaishir ophiolite are more evolved than low-Ca and high-Ca boninites from the IBM system and additionally display a calc-alkaline signature in the AFM-space.

A careful comparison with boninites (Reagan et al. 2015) and tholeiitic basalts (Reagan et al. 2010; Arculus et al. 2015) dredged along the IBM system shows that major elements and V for crustal rocks of the Khantaishir ophiolite overlap the rocks of the boninite series recovered during IODP Expeditions 352 at sites U1439 and U1442 (Fig. 8), while Zr shows a marked depletion. Additionally, the boninite series of the IBM system is characterized by a high abundance of evolved rocks (referred as high-Mg andesites, Reagan et al. 2015), a feature that is noticed also in the Khantaishir ophiolite, where the andesitic suite represents the majority of the analyzed rocks. Moreover, Fig. 8 clearly shows that tholeiitic basalts collected behind the Izu-Bonin arc during Expedition 351 at site U1438 (Arculus et al. 2015) and those collected in the forearc of the Mariana arc (referred as forearc basalts or FAB, Reagan et al. 2010) have distinct chemical compositions, both in major and trace elements, compared to the rocks of the Khantaishir ophiolite. Figure 8 also shows that the volcanic rocks of the Khantaishir ophiolite have analogous major and trace element concentrations as transitional lavas (i.e. lavas occurring between FAB and boninites) of the IBM system (Reagan et al. 2010). However, the transitional lavas from IBM are characterized by lower MgO.

Trace element patterns and anomalies in the IBM boninites and tholeiitic basaltic-andesites to andesites of the Khantaishir crust indicate a moderate but clearly identifiable subduction component (Fig. 7a–c). More primitive ($X_{Mg} > 0.70$) samples from the Khantaishir ophiolite are depleted compared to low-Ca boninites from the Izu-Bonin

arc, except for their middle- and heavy-REE, which show similar concentrations. Primitive to slightly fractionated samples ($0.60 < X_{Mg} < 0.70$) have comparable LILE concentrations, negative Nb anomalies and positive anomalies for Pb and Sr as low-Ca boninites from IBM. However, low-Ca boninites show a depletion in REE, with the typical "spoon-shaped pattern", a characteristic that is not observed in the rocks of the Khantaishir ophiolite. Moreover, for the rocks of Khantaishir it is possible to observe that they have HFSE and REE depleted compared to FAB dredged in the Mariana forearc. Evolved rocks ($X_{Mg} < 0.60$) from the Khantaishir crust, represented by the high-Mg andesites of the andesitic suite, have LILE concentrations similar to FAB, but most samples also display a marked depletion in HFSE and REE. Moreover, the low-X_{Mg} rocks of the Khantaishir ophiolite have a primitive mantle normalized pattern nearly identical to the transitional lavas of the IBM system. Nevertheless, the lithologies of the Khantaishir ophiolite have stronger Nb-negative anomalies and higher concentrations in La and Ce than the transitional lavas. A single analysis (sample KT11-98, $X_{Mg} = 0.38$) has a REE normalized pattern similar to FAB. However, this feature and its high TiO_2 concentration (1.2 wt%) are consistent with a composition akin to an evolved tholeiitic island arc basalt. In general, HREE-concentrations of the Khantaishir crustal rocks indicate a mantle source more depleted than the source for MOR basalts or FAB, but slightly enriched compared to low-Ca boninites from the Izu-Bonin arc. Furthermore, variations in Ti/V, Th–Nb–Yb and Ba/Th (see Online Resource 7a–d) emphasize the different chemical composition between crustal rocks of the Khantaishir ophiolite and FAB. These diagrams also indicate that transitional lavas from the IBM system are similar, but not identical, to volcanic rocks from the Khantaishir ophiolite, since they have higher Rb/Nb ratios and plot closer to the MORB-OIB array than Khantaishir lavas.

Ophiolites

The Khantaishir ophiolite is chemically distinct from other Mongolian ophiolites that are MORB-like (e.g. Bayankhongor, Kepezhinskas et al. 1991; Terent'eva et al. 2008). The crustal rocks of the Khantaishir ophiolite are quartz normative as the lavas from the tholeiitic series (Regelous et al. 2014) and those from the boninitic series (König et al. 2008) of the Troodos ophiolite (Fig. 9). However, in terms of major and trace element compositions, the tholeiitic lavas from Troodos have lower SiO_2 and Na_2O concentrations, and higher CaO, TiO_2, Zr and (for some samples) V concentrations compared to the Khantaishir (Figs. 5a–f, 6a–f). Additionally, Ti/V ratios (Online Resource 7a–d) for the Troodos tholeiitic series follow a trend comparable with that recognized in FAB, highlighting again the

difference with Khantaishir lavas. On the other hand, the lavas from the boninitic series of Troodos overlap the analyses of the Khantaishir ophiolite. Troodos has been often designated as subduction-related (Miyashiro 1973; Portnyagin et al. 1997; Pearce and Robinson 2010). In particular, the Upper Pillow Lavas unit in the Troodos ophiolite is a reference example for high-Ca boninites, a sub-group of boninites characterized by cpx-phenocrysts, as well as cpx + plag in the groundmass (Cameron 1985; Crawford et al. 1989; König et al. 2008). The progression from tholeiitic lavas to more boninitic-like lavas has recently led to the hypothesis that the Troodos ophiolite may have been formed at a spreading center close to a ridge-trench-trench or a ridge-trench-transform triple junction (Regelous et al. 2014). By contrast in the Oman ophiolite, boninites are minor and occur in the northern part of the ophiolite, within the Alley volcanic unit. This unit covers the Geotimes/V1 extrusive rocks, which have a typical signature of spreading-ridge-derived lavas (Ishikawa et al. 2002), forming an architecture that is very akin to the one observed in the Troodos ophiolite. Note that, as for the Troodos ophiolite (e.g. Regelous et al. 2014), the setting of the Oman ophiolite is still controversial (e.g. Pearce et al. 1981; Searle and Cox 1999; Nicolas and Boudier 2015).

The above-mentioned similarities and dissimilarities are confirmed by a statistical comparison with the East Pacific Rise (EPR), the Mariana backarc basin, the boninites from the IBM system and the ophiolites of Oman and Troodos (Online Resource 8a–h). Further comparison with other supra-subduction-related ophiolites such as Bay of Islands and Betts Cove (Newfoundland) indicates that the Khantaishir ophiolite differs from the Bay of Islands ophiolite because this latter shows a complete transition from non-arc- to arc-related signatures (Jenner et al. 1991); as observed in the Troodos ophiolite (Regelous et al. 2014) and along the IBM system (e.g. Ishizuka et al. 2011; Arculus et al. 2015; Reagan et al. 2015). Moreover, the arc-related lavas of the Bay of Islands ophiolite display trace element normalized patterns which are enriched compared to those of the Khantaishir ophiolite (Jenner et al. 1991). On the other hand, boninites of the Betts Cove ophiolite (Bédard 1999) are comparable, both in term of major and trace elements (Online Resource 3) to the volcanics of the Khantaishir. It is interesting to note that in the Betts Cove ophiolite there is a systematic progression of the magmatism from boninitic to arc-tholeiitic (Bédard 1999), suggesting a more focused volcanism similar to that observed in the Khantaishir ophiolite.

From this comparison it appears that some ophiolites (Troodos, Oman, Bay of Islands) preserve a whole transition from arc-unrelated to arc-related lavas, whereas other ophiolites (Khantaishir and Betts Cove) are characterized only by the presence of arc-related lavas (as also reviewed, e.g. in Dilek and Furnes 2014).

The Khantaishir ophiolite: incipient arc crust

High SiO_2 concentrations at high X_{Mg} (mostly > 0.60), elevated LILE and distinct trace element anomalies, early crystallization of amphibole and suppression of plagioclase all indicate that the Khantaishir was derived by low-pressure, H_2O-assisted melting of a mantle modified by a hydrous subduction component. The relative low Ca-concentrations and highly depleted HREE require this mantle to be strongly depleted.

The Khantaishir ophiolite displays arc crust over 113 km^2 and its crust-mantle transition over 31 km without any evidence of pre-existing crust. Although the Khantaishir ophiolite preserves an architecture comparable with that observed at mid-oceanic ridges, the main difference is the absence of a classical vertical sheeted dyke complex, which is replaced by a section composed of dykes and sills (similar to the igneous basement observed in U1339 and U1440 drilling sites of the IBM system, Reagan et al. 2015). The general dip of 50°–60° observed in the dykes of the dykes + sills complex possibly indicate that these dykes were rotated due to rapid subsidence during crustal thickening or tectonic faulting above the main locus of magmatism, as suggested by Karson et al. (1992) for similarly inclined dykes near the Hess Deep spreading ridge.

Furthermore, the SiO_2-rich, TiO_2-poor and HREE-depleted boninitic to high-Mg andesitic lavas from the Khantaishir complex strongly differ from typical MOR basalts or backarc basalts, but also from forearc basalts (FAB) dredged in the IBM system. This latter aspect is of particular importance because the typical stratigraphy observed in the IBM system shows FAB at the bottom, overlain by transitional lavas and boninites, which in turn are covered by high-Mg andesites, reflecting a progressive transition from lavas with a minor slab input to lavas formed during a more focused (arc-related) stage of magmatism (e.g. Reagan et al. 2010, 2015; Ishizuka et al. 2011). In the Khantaishir ophiolite, the absence of pre-existing FAB (or any previous oceanic crust), and the widespread occurrence of boninites and high-Mg andesites with a chemical signature comparable with IBM-transitional lavas, indicate that subduction initiation begun with an already focused volcanism during the incipient stage of arc magmatism. The focused volcanism seems also to be supported by the evidence that boninites and high-Mg andesites occur irregularly distributed within the stratigraphic sequence, without showing any particular stratification (see Online Resource 4). The resulting crust represents hence the first one built on a completely denudated mantle. The top units are pillows extruded into water and in part covered by (Neoproterozoic–Cambrian) marine sediments supporting formation in a marine environment, pillows also occur directly on the mantle. The presence of pillow lavas directly on mantle rocks suggests that these lavas may represent the very first melts that rose immediately towards the surface and were emplaced onto the denudated mantle during early stages of incipient arc-magmatism, before a lower gabbroic cumulate sequence could be formed. Volcanic edifices, as would be characteristic for well-developed arcs, are not observed. Nevertheless, the volcanoclastics which are stratigraphically on top of the Khantaishir pillows have major and trace element compositions similar to the other volcanics and may represent the first occurrence of sub-aerial volcanism. Yet, the age of the volcanoclastics is unknown and their relation to the ophiolite only putative.

In the intra-oceanic Izu-Bonin-Mariana system, boninitic volcaniclastics are the incipient arc products deposited on pre-existing MOR-type basaltic oceanic crust (Reagan et al. 2010; Ishizuka et al. 2011). Deep sea drilling (Arculus et al. 2015) and dredging (Ishizuka et al. 2006) have shown that boninites and basalts with a comparable slab signature and of similar age (52–48, Ishizuka et al. 2014) are the oldest volcanic arc-related products in the area and either are interbedded with thin layers of deep sea sediments (Ishizuka et al. 2006) or form the cover of the igneous basement below late Eocene sediments (Arculus et al. 2015). The stratigraphy of the drill cores allows a clear attribution of the boninites to incipient arc-formation. The highly depleted high-Mg andesites or boninites from the Bonin (or Ogasawara) Islands also formed at 48–44 Ma (Ishizuka et al. 2014), shortly after the IBM subduction system started around 52–50 Ma. Most likely, the Bonin Islands were part of the main arc in the Eocene; their present day forearc position does not inform on the tectonic situation 50 Ma ago, in particular as the Bonin Islands formed ~ 3000 km South of the present day position (Seno and Maruyama 1984). Altogether, magmatism related to incipient arc crust formation in the IBM system starts with boninitic compositions (e.g. Reagan et al. 2010, 2015; Ishizuka et al. 2011; Stern et al. 2012) and drill cores, dredges and the Bonin Islands allow to reconstruct the history of the early IBM magmatism. The Khantaishir offers complementary information as it provides an almost unique opportunity to study the architecture of such initial arc crust.

As a word of caution, boninites per se are not an exclusive feature of incipient arc magmatism; petrologically, they simply result from shallow, H_2O-assisted melting of a highly depleted mantle combined with a minor slab component (that also provides the H_2O). Such a combination is also realized in the northern Tonga arc: There, boninites are only a few Ma old and occur in a rear-arc position where a Lau basin backarc spreading center interferes with the northern end of the Tonga arc itself (Resing et al. 2011).

The geochemistry of the Khantaishir is very much analogous to the boninites that characterize the initiation of magmatism in the intra-oceanic Izu-Bonin-Mariana arc. The lack of pre-existing crust on the Khantaishir mantle lends strong

support that the Khantaishir crust represents a novel episode of subduction-related magmatism in the area, in all likelihood resulting from subduction initiation. It should further be noted that MORB-like oceanic crust is also rare (or possibly absent) in the two intra-oceanic paleo-arcs where a complete section is exposed (Kohistan and Talkeetna, e.g. Jagoutz and Kelemen 2015), possibly indicating that mantle denudation might be a general feature of intra-oceanic subduction initiation. All these findings suggest that subduction initiation may start with an already (focused) arc-style magmatism, a mechanism that slightly differ from what observed in the IBM subduction system, where the very earliest lavas produced during decompression melting are MORB-like forearc basalts (e.g. Reagan et al. 2010, 2015; Ishizuka et al. 2011; Arculus et al. 2015). Nevertheless, this incipient arc magmatism is in excellent agreement with the models of Stern and Bloomer (1992) and of Shervais (2001) where spontaneous subduction initiation starts with the sinking of heavy oceanic lithosphere, probably along fracture zones, that separates two oceanic plates with different ages. The sinking leads to an extensional regime where asthenospheric mantle from below the future overriding plate fills the resulting "gap" (Fig. 10a–c). The resulting upwelling of the asthenosphere into the future mantle wedge then results in adiabatic decompression melting, boosted by minor fluxing with slab fluids. The interaction of these two effects favors the production of low pressure H_2O-bearing melts with an arc-signature, such as boninites.

Conclusions

The high-Si Khantaishir ophiolite strongly differs in composition from melts generated in backarc basins or along mid-ocean ridges and lacks the typical vertical sheeted dykes complex observed within the oceanic crust. Geochemically, the Khantaishir volcanics were generated in a supra-subduction environment and correspond well to boninites and high-Mg andesites that characterize subduction initiation in the IBM arc.

Some of the most important conclusions drawn from the Khantaishir ophiolite derive from what is not observed: there is a complete lack of pre-existing crust, no evidence for volcanic edifices and no major faults where pillows and mantle are in direct contact. Together, this results in a scenario where a nascent oceanic arc crust is formed on denudated mantle. The major element geochemistry suggests a shallow H_2O-assisted melting regime, possibly at as little as 15 km depth.

The role of a heavily depleted mantle for intra-oceanic arc initiation remains a vexing question. In the western Pacific, the IBM arc initiated with boninites derived from an ultra-depleted mantle; the same is observed in
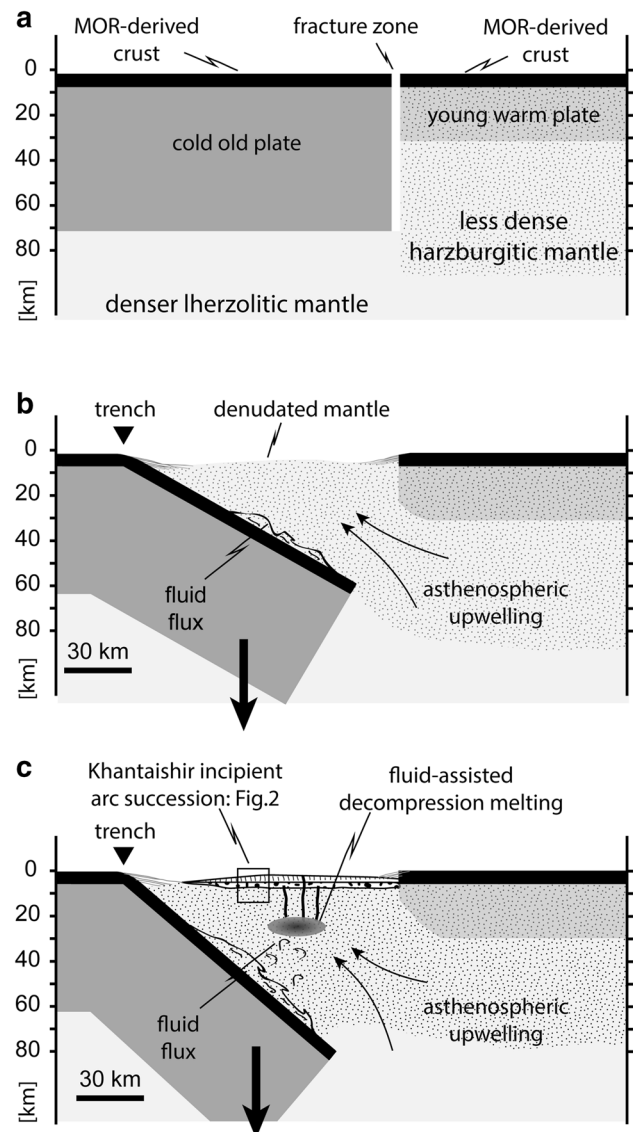

Fig. 10 Model for subduction initiation and formation of the Khantaishir incipient arc succession

the Khantaishir and Betts Cove ophiolites. Possibly, this could be a mere coincidence. Not believing in coincidences we note that the lateral density contrast between a younger lighter and an older denser lithosphere is amplified if the mantle of the younger plate is highly depleted ($\rho^{harzburgite}$ = 3.1–3.2 g/cm^3) and the mantle of the older plate fertile ($\rho^{lherzolite}$ = 3.2–3.3 g/cm^3). One may even speculate that a mantle fertility contrast across a major fault may already provide the kind of discontinuity necessary to start the sinking and then subduction of the heavier lithosphere, although a combination of age and fertility difference results in the maximum density contrast. The lighter harzburgitic mantle from the future overriding plate will then intrude into the future mantle wedge, yielding a

plausible causal link between subduction initiation and an early suite of boninitic melts.

References

Arculus RJ, Ishizuka O, Bogus KA, Gurnis M, Hickey-Vargas R, Aljahdali MH, Bandini-Maeder AN, Barth AP, Brandl PA, Drab L, do Monte Guerra R, Hamada M, Jiang F, Kanayama K, Kender S, Kusano Y, Li H, Loudin LC, Maffione M, Marsaglia KM, McCarthy A, Meffre S, Morris A, Neuhaus M, Savov IP, Sena C, Tepley FJ, Van der Land C, Yogodzinski GM, Zhang Z (2015) A record of spontaneous subduction initiation in the Izu-Bonin-Mariana arc. Nat Geosci 8:728–733

Badarch G, Cunningham WD, Windley BF (2002) A new terrane subdivision for Mongolia: implications for the Phanerozoic crustal growth of Central Asia. J Asian Earth Sci 21:87–110

Bédard JH (1999) Petrogenesis of boninites from the Betts Cove ophiolite, Newfoundland, Canada: identification of subducted source components. J Petrol 40:1853–1889

Bold U, Smith EF, Rooney AD, Bowring SA, Buchwaldt R, Dudás FŐ, Ramezani J, Crowley JL, Schrag DP, MacDonald FA (2016) Neoproterozoic stratigraphy of the Zavkhan terrane of Mongolia: the backbone for Cryogenian and early Ediacaran chemostratigraphic records. Am J Sci 316:1–63

Bucholz CE, Jagoutz O, Schmidt MW, Sambuu O (2014) Phlogopite- and clinopyroxene-dominated fractional crystallization of an alkaline primitive melt: petrology and mineral chemistry of the Dariv Igneous Complex, Western Mongolia. Contrib Mineral Petrol 167:1–28

Cameron WE (1985) Petrology and origin of primitive lavas from the Troodos ophiolite, Cyprus. Contrib Mineral Petrol 89:239–255

Conference Participants (1972) Penrose field conference on ophiolites. Geotimes 17:24–25

Cooper LB, Plank T, Arculus RJ, Hauri EH, Hall PS, Parman SW (2010) High-Ca boninites from the active Tonga Arc. J Geophys Res 115:1–23

Cosca MA, Arculus RJ, Pearce JA, Mitchell JG (1998) $^{40}Ar/^{39}Ar$ and K–Ar geochronological age constraints for the inception and early evolution of the Izu–Bonin–Mariana arc system. Island Arc 7:579–595

Crawford AJ, Falloon TJ, Green DH (1989) Classification, petrogenesis and tectonic setting of boninites. In: Crawford AJ (ed) Boninites. Unwin Hyman, London, p 465

Crisp JA (1984) Rates of magma emplacement and volcanic output. J Volcanol Geotherm Res 20:177–211

Delor C, Deroin JP, Maluski H, Tomurtogoo O (2000) Petrostructural constraints and Ar–Ar dating of the Bayankhongor ophiolites. In: Badarch G, Jahn BM (eds) IGCP 420 Continental growth in the Phanerozoic: evidence from Central Asia, Second workshop, abstracts and excursion guidebook (Geotraverse through a terrane collage in southern Hangay) July 25–August 3, 1999, Ulaanbaatar, Mongolia. Geosciences Rennes, hors serie n. 2, Rennes

Dilek Y, Furnes H (2014) Ophiolites and their origins. Elements 10:93–100

Gaetani GA, Grove TL, Bryan WB (1993) The influence of water on the petrogenesis of subduction-related igneous rocks. Nature 365:332–334

Gibsher AS, Khain EV, Kotov AB, Sal'nikova EV, Kozakov IK, Kovach VP, Yakovleva SZ, Fedoseenko AM (2001) Late Vendian age of the Han-Taishiri ophiolite complex in western Mongolia. Rus Geol Geophys 42:1110–1117

Gillis KM, Banerjee NR (2000) Hydrothermal alteration patterns in supra-subduction zone ophiolites. Geol Soc Am 349:283–297

Guillong M, Meier DL, Allan MM, Heinrich CA, Yardley BWD (2008) A MATLAB-based program for reduction of laser ablation ICP-MS data of homogeneous material and inclusions. In: Sylvester P (ed) Laser ablation ICP-MS in the earth sciences: current practices and outstanding issues, vol 40. Mineralogical Association of Canada Short Course, Vancouver, pp 328–333

Gurnis M, Hall C, Lavier L (2004) Evolving force balance during incipient subduction. Geochem Geophys Geosyst 5:1–31

Hickey RL, Frey FA (1982) Geochemical characteristics of boninite series volcanics: implications for their source. Geochim Cosmochim Acta 46:2099–2115

Ishikawa T, Nagaishi K, Umino S (2002) Boninitic volcanism in the Oman ophiolite: implications for thermal condition during transition from spreading ridge to arc. Geology 30:899–902

Ishizuka O, Kimura JI, Li YB, Stern RJ, Reagan MK, Taylor RN, Ohara Y, Bloomer SH, Ishii T, Hargrove US, Haraguchi S (2006) Early stages in the evolution of Izu–Bonin arc volcanism: new age, chemical and isotopic constraints. Earth Planet Sci Lett 250:385–401

Ishizuka O, Tani K, Reagan MK, Kanayama K, Umino S, Harigane Y, Sakamoto I, Miyajima Y, Yuasa M, Dunkley DJ (2011) The timescales of subduction initiation and subsequent evolution of an oceanic island arc. Earth Planet Sci Lett 306:229–240

Ishizuka O, Tani K, Reagan MK (2014) Izu-Bonin-Mariana forearc crust as a modern ophiolite analogue. Elements 10:115–120

Jagoutz O, Kelemen PB (2015) Role of arc processes in the formation of continental crust. Annu Rev Earth Planet Sci 43:363–404

Jenner GA, Dunning GR, Malpas J, Brown M, Brace T (1991) Bay of Islands and little port complexes, revisited: age, geochemical and isotopic evidence confirm suprasubduction-zone origin. Can J Earth Sci 28:1635–1652

Jian P, Kröner A, Jahn B, Windley BF, Shi Y, Zhang W, Zhang F, Miao L, Tomurhuu D, Liu D (2014) Zircon dating of Neoproterozoic and Cambrian ophiolites in West Mongolia and implications for the timing of orogenic processes in the central part of the Central Asian Orogenic Belt. Earth Sci Rev 133:62–93

Karson JA, Hurst SD, Lonsdale P (1992) Tectonic rotation of dikes in fast-spread oceanic crust near Hess Deep. Geology 20:685–688

Kelemen PB, Hanghøj K, Greene AR (2003) One view of the geochemistry of subduction-related magmatic arcs, with an emphasis on primitive andesite and lower crust. In: Holland HD, Turekian KK (eds) Treatise on geochemistry, vol 3. Elsevier, pp 1–70

Kelley KA, Cottrell E (2009) Water and the oxidation state of subduction zone magmas. Science 325:605–607

Kepezhinskas PK, Kepezhinskas KB, Pukhtel IS (1991) Lower Paleozoic oceanic crust in Mongolian Caledonides: Sm–Nd isotope and trace element data. Geophys Res Lett 18:1301–1304

König S, Münker C, Schuth S, Garbe-Schönberg D (2008) Mobility of tungsten in subduction zones. Earth Planet Sci Lett 274:82–92

Kozakov IK, Sal'nikova EB, Khain EV, Kovach VP, Berezhnaya NG, Yakovleva SZ, Plotkina YV (2002) Early Caledonian crystalline rocks of the lake zone in Mongolia: formation history and tectonic settings as deduced from U–Pb and Sm–Nd datings. Geotectonics 36:156–166

Le Bas MJ (2000) IUGS reclassification of the high-Mg and picritic volcanic rocks. J Petrol 41:1467–1470

Li C, Ripley EM (2010) The relative effects of composition and temperature on olivine-liquid Ni partitioning: statistical deconvolution and implications for petrologic modeling. Chem Geol 275:99–104

Matsumoto I, Tomurtogoo O (2003) Petrological characteristics of the Hantaishir ophiolite complex, Altai Region, Mongolia: coexistence of podiform chromitite and boninites. Gondwana Res 6:161–169

McDonough WF, Sun SS (1995) The composition of the Earth. Chem Geol 120:223–253

Miyashiro A (1973) The Troodos ophiolitic complex was probably formed in an island arc. Earth Planet Sci Lett 19:218–224

Nicolas A, Boudier F (2015) Structural contribution from the Oman ophiolite to processes of crustal accretion at the East Pacific Rise. Terra Nova 27:77–96

Pearce JA, Robinson PT (2010) The Troodos ophiolitic complex probably formed in a subduction initiation, slab edge setting. Gondwana Res 18:60–81

Pearce JA, Alabaster T, Shelton AW, Searle MP (1981) The Oman ophiolite as a cretaceous arc-basin complex: evidence and implications. Philos Trans R Soc Lond 300:299–317

Pearce JA, Van der Laan SR, Arculus RJ, Murton BJ, Ishii T, Peate DW, Parkinson IJ (1992) Boninite and harzburgite from Leg 125 (Bonin-Mariana forearc): a case study of magma genesis during the initial stages of subduction. Pac Ocean Drill Prog Sci Res 125:623–659

Peccerillo A, Taylor SR (1976) Geochemistry of Eocene calc-alkaline volcanic rocks from the Kastamonu area, northern Turkey. Contrib Mineral Petrol 58:63–81

Portnyagin MV, Danyushevsky LV, Kamenetsky VS (1997) Coexistence of two distinct mantle sources during formation of ophiolites: a case study of primitive pillow-lavas from the lowest part of the volcanic section of the Troodos ophiolite, Cyprus. Contrib Mineral Petrol 128:287–301

Putirka KD (2008) Thermometers and barometers for volcanic systems. Rev Miner Geochem 69:61–120

Reagan MK, Ishizuka O, Stern RJ, Kelley KA, Ohara Y, Blichert-Toft J, Bloomer SH, Cash J, Fryer P, Hanan BB, Hickey-Vargas R, Ishii T, Kimura J-I, Peate DW, Rowe MC, Woods M (2010) Fore-arc basalts and subduction initiation in the Izu-Bonin-Mariana system. Geochem Geophys Geosyst 11:1–17

Reagan MK, Pearce JA, Petronotis K, Almeev R, Avery AA, Expedition 352 Scientists (2015) Izu-Bonin-Mariana fore arc: testing subduction initiation and ophiolite models by drilling the outer Izu-Bonin-Mariana fore arc. Int Ocean Disc Prog Prelim Rep 352:1–86

Regelous M, Haase KM, Freund S, Keith M, Weinzierl CG, Beier C, Brandl PA, Endres T, Schmidt H (2014) Formation of the Troodos ophiolite at a triple junction: evidence from trace elements in volcanic glass. Chem Geol 386:66–79

Resing JA, Rubin KH, Embley RW, Lupton JE, Baker ET, Dziak RP, Baumberger T, Lilley MD, Huber JA, Shank TM, Butterfield DA, Clague DA, Keller NS, Merle SG, Buck NJ, Michael PJ, Soule A, Caress DW, Walker SL, Davis R, Cowen JP, Reysenbach AL, Thomas H (2011) Active submarine eruption of boninite in the northeastern Lau basin. Nat Geosci 4:799–806

Robinson PT, Melson WG, O'Hearn T, Schmincke HU (1983) Volcanic glass compositions of the Troodos ophiolite, Cyprus. Geology 11:400–404

Roeder PL, Emslie RF (1970) Olivine-liquid equilibrium. Contrib Mineral Petrol 29:275–289

Ruzhentsev SV, Burashnikov VV (1996) Tectonics of the western Mongolian Salairides. Geotectonics 29:379–394

Searle M, Cox J (1999) Tectonic setting, origin, and obduction of the Oman ophiolite. Geol Soc Am Bull 111:104–122

Şengör AMC, Natal'in BA, Burtman VS (1993) Evolution of the Altaid tectonic collage and Palaeozoic crustal growth in Eurasia. Nature 364:299–307

Seno T, Maruyama S (1984) Paleogeographic reconstruction and origin of the Philippine Sea. Tectonophysics 102:53–84

Shervais JW (2001) Birth, death, and resurrection: the life cycle of suprasubduction zone ophiolites. Geochem Geophys Geosyst 2:1–45

Sisson TW, Grove TL (1993) Experimental investigations of the role of H_2O in calc-alkaline differentiation and subduction zone magmatism. Contrib Mineral Petrol 113:143–166

Stern RJ (2004) Subduction initiation: spontaneous and induced. Earth Planet Sci Lett 226:275–292

Stern RJ, Bloomer SH (1992) Subduction zone infancy: examples from the Eocene Izu-Bonin-Mariana and Jurassic California arcs. Geol Soc Am Bull 104:1621–1636

Stern RJ, Fouch MJ, Klemperer SL (2003) An overview of the Izu-Bonin-Mariana subduction factory. In: Eiler J (ed) Inside the subduction factory, Geophysical Monograph 138. American Geophysical Union, Washington D.C., pp 175–222

Stern RJ, Reagan M, Ishizuka O, Ohara Y, Whattam S (2012) To understand subduction initiation, study forearc crust: to understand forearc crust, study ophiolites. Lithosphere 4:469–483

Sun S-S, McDonough WS (1989) Chemical and isotopic systematics of oceanic basalts: implications for mantle composition and processes. Geol Soc Lond Spec Publ 42(1):313–345

Tatsumi Y, Suzuki T (2009) Tholeiitic vs calc-alkalic differentiation and evolution of arc crust: constraints from melting experiments on a basalt from the Izu-Bonin-Mariana arc. J Petrol 50:1575–1603

Terent'eva LB, Kovach VP, Yarmolyuk VV, Kovalenko VI, Kozlovsky AM (2008) Composition, sources, and geodynamics of rock formation in the Late Riphean Bayankhongor ophiolite zone: characteristics of early stages in the evolution of the Paleo-Asian Ocean. Doklady Earth Sci 423A:1462–1466

Ulmer P (2001) Partial melting in the mantle wedge—the role of H_2O in the genesis of mantle-derived "arc-related" magmas. Phys Earth Planet Int 127:215–232

Umino S, Kushiro I (1989) Experimental studies on boninite petrogenesis. In: Crawford AJ (ed) Boninites. Unwin Hyman, London, p 465

Van der Laan SR, Flower MFJ, Van Groos AFK (1989) Experimental evidence for the origin of boninites: near-liquidus phase relations to 7.5 kbar. In: Crawford AJ (ed) Boninites. Unwin Hyman, London, p 465

Walker DA, Cameron WE (1983) Boninite primary magmas: evidence from the Cape Vogel Peninsula, PNG. Contrib Mineral Petrol 83:150–158